ORIGINAL ARTICLE

JBMR®

# Functional Scaffold-Free Bone Equivalents Induce Osteogenic and Angiogenic Processes in a Human In Vitro Fracture Hematoma Model

Moritz Pfeiffenberger,[1,2] Alexandra Damerau,[1,2] Igor Ponomarev,[3] Christian H Bucher,[4,5] Yuling Chen,[1,2] Dirk Barnewitz,[3] Christa Thöne-Reineke,[6] Paula Hoff,[1,7] Frank Buttgereit,[1,2,4] Timo Gaber,[1,2,4] and Annemarie Lang[1,2,4]

[1]Department of Rheumatology and Clinical Immunology, Charité – Universitätsmedizin Berlin, Corporate Member of Freie Universität Berlin, Humboldt-Universität zu Berlin, and Berlin Institute of Health, Berlin, Germany
[2]German Rheumatism Research Centre (DRFZ) Berlin, a Leibniz Institute, Berlin, Germany
[3]Research Center of Medical Technology and Biotechnology, Bad Langensalza, Germany
[4]Charité – Universitätsmedizin Berlin, Corporate Member of Freie Universität Berlin, Humboldt-Universität zu Berlin, and Berlin Institute of Health, Berlin Institute of Health Center for Regenerative Therapies, Berlin, Germany
[5]Charité – Universitätsmedizin Berlin, Corporate Member of Freie Universität Berlin, Humboldt-Universität zu Berlin, and Berlin Institute of Health, Julius Wolff Institute, Berlin, Germany
[6]Institute of Animal Welfare, Animal Behavior, and Laboratory Animal Science, Department of Veterinary Medicine, Freie Universität Berlin, Berlin, Germany
[7]Endokrinologikum Berlin, MVZ am Gendarmenmarkt, Berlin, Germany

## ABSTRACT

After trauma, the formed fracture hematoma within the fracture gap contains all the important components (immune/stem cells, mediators) to initiate bone regeneration immediately. Thus, it is of great importance but also the most susceptible to negative influences. To study the interaction between bone and immune cells within the fracture gap, up-to-date in vitro systems should be capable of recapitulating cellular and humoral interactions and the physicochemical microenvironment (eg, hypoxia). Here, we first developed and characterized scaffold-free bone-like constructs (SFBCs), which were produced from bone marrow–derived mesenchymal stromal cells (MSCs) using a macroscale mesenchymal condensation approach. SFBCs revealed permeating mineralization characterized by increased bone volume (μCT, histology) and expression of osteogenic markers (*RUNX2, SPP1, RANKL*). Fracture hematoma (FH) models, consisting of human peripheral blood (immune cells) mixed with MSCs, were co-cultivated with SFBCs under hypoxic conditions. As a result, FH models revealed an increased expression of osteogenic (*RUNX2, SPP1*), angiogenic (*MMP2, VEGF*), HIF-related (*LDHA, PGK1*), and inflammatory (*IL6, IL8*) markers after 12 and 48 hours co-cultivation. Osteogenic and angiogenic gene expression of the FH indicate the osteoinductive potential and, thus, the biological functionality of the SFBCs. IL-6, IL-8, GM-CSF, and MIP-1β were detectable within the supernatant after 24 and 48 hours of co-cultivation. To confirm the responsiveness of our model to modifying substances (eg, therapeutics), we used deferoxamine (DFO), which is well known to induce a cellular hypoxic adaptation response. Indeed, DFO particularly increased hypoxia-adaptive, osteogenic, and angiogenic processes within the FH models but had little effect on the SFBCs, indicating different response dynamics within the co-cultivation system. Therefore, based on our data, we have successfully modeled processes within the initial fracture healing phase in vitro and concluded that the cross-talk between bone and immune cells in the initial fracture healing phase is of particular importance for preclinical studies. © 2021 The Authors. *Journal of Bone and Mineral Research* published by Wiley Periodicals LLC on behalf of American Society for Bone and Mineral Research (ASBMR)..

**KEY WORDS:** BIOENGINEERING; FRACTURE HEALING; FRACTURE HEMATOMA; OSTEOIMMUNOLOGY



Received in original form July 24, 2020; revised form January 20, 2021; accepted January 29, 2021. Accepted manuscript online February 3, 2021.

Address correspondence to: Annemarie Lang, PhD, Department of Rheumatology and Clinical Immunology, Charité – Universitätsmedizin Berlin, Corporate Member of Freie Universität Berlin, Humboldt-Universität zu Berlin, and Berlin Institute of Health, Charitéplatz 1, 10117 Berlin, Germany. E-mail: annemarie.lang@charite.de

Additional Supporting Information may be found in the online version of this article.

Journal of Bone and Mineral Research, Vol. 36, No. 6, June 2021, pp 1189–1201.
DOI: 10.1002/jbmr.4267

## Introduction

Bone pathologies such as osteoporosis or disturbed fracture healing lead to pain, immobility, inflexibility, considerable loss of life quality, and even mental illnesses.[1] Traumatic events can result in bone fracturing accompanied by vessel ruptures and the opening of the bone marrow channel. An important event in the initial phase of fracture healing is the formation of the fracture hematoma, which mainly consists of immune and chondro- and osteoprogenitor cells.[2,3] Negative influences such as medications or comorbidities including diabetes, rheumatoid arthritis, or immunosuppression can lead to dysregulation within the inflammatory phase of fracture healing and to impairments within the following regeneration process.[4,5] Recent treatment strategies have achieved high-technology standards with regard to fixation systems such as plates or implants, regenerative approaches using autologous bone graft (gold standard), or the additional application of stem cells and/or growth factors.[6] Therefore, preclinical studies are highly needed to tackle the unmet clinical need, especially with respect to an aging population and the increase of comorbidities.

The surgical removal of the fracture hematoma results in a prolonged healing process, whereas transplantation in an ectopic location leads to endochondral bone formation at the implantation site.[7] Formation of the fracture hematoma and the constricted interplay of pro- and anti-inflammatory processes are considered as the starting point of bone regeneration.[8] Because the bone marrow cavity is opened during the fracture, the bone marrow acts as a resource for immune cells as well as chondro- and osteoprogenitor cells such as mesenchymal stromal cells (MSCs). Therefore, it can be hypothesized that osteogenic induction within the fracture gap is directly induced and controlled by signals from bone components in the vicinity of the fracture gap.[9,10] Hence, the cross-talk between immune cells from peripheral blood (after vessel rupture) and the bone marrow and osteoprogenitor cells is essential and needs to be considered in preclinical studies.[11] Today's gold standard of preclinical drug, compound screening, and risk assessment is the use of animal models—mainly rodents (mice and rats)—which is in accordance with most national legal requirements. Nevertheless, trans-species differences may be responsible for the limited transferability of findings to the human patient.[12] Mimicking the in-patient situation in preclinical studies is highly encouraged and evading cross-species differences by novel in vitro approaches is of great interest. During the past decades, conventional in vitro cell culture systems have been revised and improved to provide more physiological and human-relevant features. Furthermore, the rapid technical evolution allocating sophisticated biomaterials, bioreactors, and microfluidic platforms allows the development of innovative human-relevant in vitro systems as alternative or predictive support to animal testing.[13]

Current in vitro systems focus on mimicking bone development, endochondral ossification, or the bone homoeostasis itself by using spheroids, scaffold-based, or scaffold-free model systems.[13] Common cell sources are either primary bone-related cells such as osteoblasts, osteocytes, osteoclasts, or MSCs as progenitor cells.[13,14] To mimic fracture healing, models mainly focus on later stages of the regeneration processes, particularly endochondral ossification or remodeling.[15] We have previously described the development of a fracture hematoma model consisting of human whole blood and a certain amount of human (h) MSCs.[16] However, to study the initiated processes in an interconnected manner and more adequate experimental setting, the combination of the bone components with the fracture hematoma (immune component) remains elusive.

Within our study, we have developed and characterized scaffold-free bone-like constructs (SFBCs) based on mesenchymal condensation, which exceeded the dimensions of spheroids. These SFBCs were co-cultivated with in vitro fracture hematoma (FH) models (i) to confirm the biological functionality of the SFBCs, and (ii) to recapitulate certain aspects of the initial phase of fracture healing allowing cell–cell interactions (immune and bone cells) and providing an adequate microenvironment (hypoxia).

## Materials and Methods

### Bone marrow–derived MSC isolation, cultivation, and characterization

Human mesenchymal stromal cells (hMSC; $n = 12$) were isolated from bone marrow of patients undergoing total hip replacement (registered and distributed by the "Tissue Harvesting" Core Facility of the Berlin Institute of Health Center for Regenerative Therapies [BCRT]; donor list in Supplemental Table S1). All protocols were approved by the Charité-Universitätsmedizin Ethics Committee and performed according to the Helsinki Declaration (ethical approval EA1/012/13). MSC isolation was performed as described in detail before.[16] Briefly, bone marrow was transferred to a 175 $cm^2$ cell culture flask, covered with expansion medium containing DMEM+GlutaMAX (Gibco, ThermoFisher, Waltham, MA, USA), 10 (v/v) % FCS (Biowest, Nuaille, France), 1 (v/v) % penicillin/streptomycin (Gibco, ThermoFisher), 20 (v/v) % StemMACS MSC Expansion Media XF (Miltenyi Biotech, Bergisch Gladbach, Germany), and incubated at 37°C in 5% $CO_2$ atmosphere (approx. 18% $O_2$). Medium was changed after 3 to 4 days when cells became adherent. Isolated cells were expanded at 37°C, 5% $CO_2$. Medium exchange was performed weekly and passaging with Trypsin–EDTA (Gibco, ThermoFisher) was conducted at a cellular confluency of 80% to 90%. For characterization, MSCs were evaluated at passage 3 for their differentiation potential (osteogenic, adipogenic) and the presence and absence of specific cell surface markers (MSC Phenotyping Kit, Miltenyi Biotech) as described in detail before.[16]

### Fabrication of the 3D bone-like scaffold-free constructs (SFBCs)

SFBCs were produced based on a patented protocol (patent no. EP1550716B1), which was modified by applying osteogenic medium to induce osteogenic differentiation after 1 week and no application of biomechanical loading to avoid matrix destruction. The osteogenic medium for generation and maturation contained DMEM/F-12, 10% (v/v) FCS, 1% (v/v) streptomycin/penicillin, 10 mM β-glycerophosphate, and 10 nM dexamethasone (all Sigma-Aldrich, St. Louis, MO, USA). Approx. 10 to 20 $\times 10^5$ hMSC/$cm^2$ (passage 3 to 4) were cultivated in expansion medium until reaching confluency and forming a closed monolayer. The cells were detached and centrifuged at 350*g* for 15 minutes at room temperature. Afterward, the resulting cell aggregates were cultivated for up to 1 week with medium exchange every day. Cell aggregates were then transferred to a 6-well plate and cultured for up to 12 weeks, enabling a

permeating mineralization of the SFBCs until performing characterization or co-cultivation with the FH model.

## Generation of FH and co-cultivation

Human EDTA blood ($n = 3$) was collected from healthy donors with written consent.[16] The FH models were generated as described previously.[16] In brief, $2.5 \times 10^5$ hMSCs were resuspended in 100 μL of EDTA-blood and subsequently mixed with a 10 mM $CaCl_2$ solution (solved in PBS). The resulting coagulate is referred to as FH. After an incubation time of 30 minutes at 37°C, 5% $CO_2$, the FH were placed on a SFBC with direct contact and cultivated in normal medium (NM) containing DMEM+GlutaMAX, 10 (v/v) % FCS, and 1 (v/v) % penicillin/streptomycin. Osteogenic medium components (OMC)—10 mM β-glycerophosphate, 0.1 mM L-ascorbic acid-2-phosphate, and 10 nM dexamethasone—were supplemented for control experiments. For the treatment study, 250 μM DFO (Sigma-Aldrich) was supplemented to the medium. The generated, combined models were incubated under hypoxic (37°C, 5% $CO_2$ and ~ 1% $O_2$, flushed with $N_2$) conditions in a humidified atmosphere for up to 48 hours.

## In vitro micro-computed tomography (μCT)

SFBCs were scanned at a nominal resolution of 8 μm, with a SkyScan 1172 high-resolution microCT (Bruker, Kontich, Belgium). X-ray tube voltage was set at 80 kV, 124 μA with maximized power of 10 W, and a 0.5 mm aluminum filter was employed to reduce beam hardening effects. The scan orbit was 360° with a rotation step of 0.2°. For reconstruction, the Bruker NRecon software accelerated by GPU was used, and Gaussian smoothing, ring artifact reduction, misalignment compensation, and beam hardening correction were applied. XY alignment was corrected with a reference scan to determine the thermal shift during scan time. The CTAn software (Bruker) was used to analyze the total volume of interest (VOI) of SFBCs. The threshold for bony tissue was set globally (determined by the Otsu method) and kept constant for all SFBCs. For analysis, we used the bone volume (BV), the bone surface (BS), and the trabecular pattern factor (TBPf)[17] as measured and calculated by the software.

## Scanning electron microscopy (SEM)

Samples were fixed with 2.5 (v/v) % glutaraldehyde (fixation for 10 minutes), dehydrated with increasing alcohol concentration 30 (v/v) % to 100 (v/v) % (5 steps), and incubated with 100% hexamethyldisilazane (all Sigma-Aldrich). Subsequently, the samples were transferred to a sample holder, and gold coating was performed with a fine gold coater JFC-1200 (JEOL, Tokyo, Japan). For electron microscopy, the JCM-6000 Plus NeoScope (JEOL) was used for imaging, and high vacuum was adjusted.

## Histological stainings

SFBCs were fixed for 6 hours in a 4 (v/v) % paraformaldehyde solution (PFA; Carl Roth, Karlsruhe, Germany) followed by an ascending sucrose solution treatment (10 [w/v] %, 20 [w/v] %, and 30 [w/v] %) for 24 hours, respectively, and afterward cryoembedded with SCEM medium (Section-lab, Hiroshima, Japan). Slices were produced with a cryotom using cryofilms (Section-lab) and afterward air-dried for 20 minutes and fixed with 4 (v/v) % PFA before every histological or immunohistological staining on a microscope slide. Hematoxylin and eosin (H&E) staining was performed as described previously.[18] In short, slices were fixed with 4 (v/v) % PFA (10 minutes), washed with distilled water, and stained with Harris's hematoxylin solution (MilliporeSigma, Burlington, MA, USA). Staining was followed by several washing steps, a differentiation step (0.25 [v/v] % concentrated HCl), and a second staining step in 0.2 (w/v) % eosin (Chroma, Waldeck, Munster, Germany). Staining was finished by differentiation in 96 (v/v) % and 100 (v/v) % ethanol, fixation with xylol, and covering with Vitro-Clud (R. Langenbrinck GmbH, Emmendingen, Germany). Alizarin Red S staining was conducted by applying slices after fixation and washing to the 2 (w/v) % Alizarin red S staining solution (Sigma-Aldrich; pH 4.1–4.3) for 10 minutes. Afterward, slices were washed in distilled water and differentiation was performed in 0.1 (v/v) % HCL solved in ethanol and fixed by washing two times with 100% ethanol before xylol fixation and covering. Von Kossa staining was conducted according to the following protocol: air drying, fixation, and washing as described above, 3% (w/v) silver nitrate solution (10 minutes), washing step with distilled water, sodium carbonate formaldehyde solution (2 minutes), washing step with tap water, 5% (w/v) sodium thiosulphate solution (5 minutes), washing step with tap water and distilled water, ascending ethanol series (70 [v/v] % to 100 [v/v] %), fixation in xylol, and covering. For Col I, II, and ALP staining, slices were rehydrated with phosphate-buffered saline (PBS) treated with 3 (v/v) % $H_2O_2$ (30 minutes), washed with PBS, blocked with 5% normal horse or goat serum (Vector Laboratories, Burlingame, CA, USA) in 2 (w/v) % bovine serum albumin (BSA), and incubated overnight with primary antibodies at 4°C (Col I antibody: ab6308, 1:500, Abcam [Cambridge, UK]; Col II antibody, 1:10, Quartett Immunodiagnostika [Berlin, Germany]; ALP antibody, ab95462, Abcam). Afterward, slices were washed and treated with 2 (v/v) % secondary antibody (biotinylated horse anti-mouse IgG antibody – Col I and Col II; biotinylated goat anti-rabbit IgG antibody – ALP, Vector Laboratories) diluted in 2 (v/v) % normal horse/goat serum/2 (v/v) % BSA/PBS (30 minutes), washed with PBS, incubated with avidin-biotin complex (Vectastain Elite ABC HRP Kit, Vector Laboratories) (50 minutes), washed with PBS, incubated with DAB under microscopic control with time measurement (DAB peroxidase (HRP) Substrate Kit, Vector Laboratories) and stopped with PBS. For counterstaining, slices were washed with distilled water and stained with Mayer's hematoxylin (Sigma-Aldrich), washed with tap water, and covered with Aquatex (MilliporeSigma). Pictures were taken with the Axioskop 40 optical microscope (Zeiss, Jena, Germany) using the corresponding AxioVision microscopy software. Von Kossa staining was quantified using ImageJ and the threshold tool to mark positive (black) and negative (brown) stained areas.

## Immunofluorescence

For the immunofluorescence staining, the slides were rehydrated with PBS and blocked with PBS with 5 (v/v) % FCS for 30 minutes at room temperature. Primary osteopontin antibody (mouse anti-human, Abcam) or osteocalcin (rabbit anti-human, Abcam) was diluted 1:50 in PBS/5 (v/v) % FCS/0.1 (v/v) % Tween 20 and incubated for 2 hours. After washing with PBS/0.1% Tween 20, the secondary antibody (donkey anti-goat A568; Life Technologies/ThermoFisher) was diluted 1:500 in PBS/5 (v/v) % FCS/0.1 (v/v) % Tween 20 and applied for 1 hour. Pictures were taken with a Keyence fluorescence microscope BZ 9000 (Keyence, Osaka, Japan) using the DAPI, TexasRed, and Cy5 channels.

### RNA isolation and quantitative PCR (qPCR)

SFBCs were transferred to RLT-buffer (Qiagen, Hilden, Germany) with 1% 2-Mercaptoethanol (Serva Electrophoresis, Heidelberg, Germany) and disrupted using the Qiagen Tissue Ruptor (Qiagen). Total RNA was extracted using the RNeasy Fibrous Tissue Mini Kit (Qiagen) according to the manufacturer's instructions, and the RNA concentration was determined using the Nanodrop ND-1000 (Peqlab, VWR International, Radnor, PA, USA). RNA was stored at −80°C until further processing. For the co-cultivation experiments, the FH and the SFBC models were analyzed separately. RNA from SFBCs was isolated as described above, and cells from the FH were dissociated by using a cell strainer (Corning, Corning, NY, USA) and washing with PBS. After centrifugation for 10 minutes at 300*g*, the cell pellet was resuspended in 350 µL RLT buffer with 3.5 µL 2-Mercaptoethanol and total RNA was extracted as described above. RNA quality was assessed via Bioanalyzer (Agilent, Santa Clara, CA, USA). cDNA was synthesized by reverse transcription using TaqMan Reverse Transcription Reagents (Applied Biosystems, Carlsbad, CA, USA) using 100 to 400 ng RNA. qPCR was performed using the DyNAmo Flash SYBR Green qPCR Kit (Thermo Fisher Scientific) and the Stratagene Mx3000P (Agilent Technologies). Initial denaturation was for 7 minutes at 98°C. Afterward, 50 cycles with 5 seconds at 98°C, 7 seconds at 56°C, and 9 seconds at 72°C were performed. The melting curve was analyzed by stepwise increasing the temperature from 50°C to 98°C every 30 seconds. All primers were designed with Primer3, verified with NCBI PrimerBlast, purchased from TIB Molbiol (Berlin, Germany), and tested for efficiency beforehand (Supplemental Table S2). *Eukaryotic translation elongation factor 1 alpha 1* (*EF1A*) was used as housekeeper gene because it has been previously reported to be stable under normoxic and hypoxic conditions.[16,19] The $2^{(-\text{delta delta C(t)})}$ method was employed to analyze the gene expression data.

### Cytokine and chemokine quantification in supernatants

Supernatants were immediately stored at −80°C after 24 and 48 hours of co-cultivation. The concentration (pg/mL) of cytokines and chemokines was determined using multiplex suspension assay (Bio-Rad Laboratories, Hercules, CA, USA) following the manufacturer's instructions. The following cytokines and chemokines (lower detection limit) were measured: IL-1β (7.55 pg/mL), IL-2 (18.99 pg/mL), IL-4 (4.13 pg/mL), IL-5 (20.29 pg/mL), IL-6 (25.94 pg/mL), IL-7 (16.05 pg/mL), IL-8 (37.9 pg/mL), IL-10 (37.9 pg/mL), IL-13 (7.21 pg/mL), IL-17 (24.44 pg/mL), interferon-gamma (IFNγ, 56.32 pg/mL), tumor necrosis factor-alpha (TNFα, 59.53 pg/mL), monocyte chemotactic protein-1 (MCP-1, 27.02 pg/mL), macrophage inflammatory protein MIP-1β (6.27 pg/mL), granulocyte colony-stimulating factor (G-CSF, 50.98 pg/mL), and granulocyte-macrophage colony-stimulating factor (GM-CSF, 11.82 pg/mL).

### Statistical analysis

Statistical tests were performed using GraphPad (La Jolla, CA, USA) Prism Software version 8. Statistical differences towards a hypothetical value were determined by the Wilcoxon signed rank test (unpaired). With respect to the co-cultivation studies, differences between two groups were determined with the Wilcoxon matched-pairs signed rank test, the Mann–Whitney test, or between more groups with the Kruskal–Wallis test with Dunn's multiple comparisons test. Probability values of $p < .05$ were considered to be statistically significant (exact $p$ values are indicated in the figures). Details on the statistics per figure are displayed in the Supplemental Information.

## Results

### SFBCs are characterized by permeating mineralization

In a first step, we wanted to know if it is possible to employ mesenchymal condensation as a macroscale approach with consistent 3D self-organization and permeating mineralization. Thus, SFBCs were generated by hMSC condensation and treatment with osteogenic medium until analysis at week 12 (Fig. 1*A*). Macroscopic observation indicated comparable generation of SFBCs from different hMSC donors with a diameter of approx. 1 cm and a thickness of 0.5 cm (Fig. 1*B*). To verify the mineralization, in vitro µCT was performed, showing a consistently high mineralization in the outer area, which was slightly reduced toward the center (Fig. 1*C*). 3D reconstruction demonstrated the presence of mineralized tissue as indicated by parameters such as bone volume (BV; mean = 5.1 ± 3.7 $mm^3$) and bone surface (BS; mean = 276.1 ± 195.4 $mm^2$) (Fig. 1*D*), however with a high standard deviation by means of the bone volume and the bone surface. To quantify the connectedness of the mineralized areas, we additionally examined the trabecular pattern factor (TBPf). This parameter was originally invented to evaluate trabecular bone. Although no osteoclasts were present in the SFBCs and thus the formation of clear trabeculae was not expected, we use this parameter to distinguish between concave (ie, connected) and convex (ie, isolated) structures. Low or even negative values represent hereby high connected tissue, which was found in at least 4 (TBPf <2) of 9 SFBCs (Fig. 1*D*). To evaluate the structural morphology of the SFBCs in further detail, we used SEM and found similar morphology when compared with human native cortical/trabecular bone (Fig. 1*E*, *F*). In detail, the top view shows strong matrix formation and a closed superficial layer with certain, isolated crystal-like depositions, while the cut face revealed a cancellous-like structure with interconnected mineralized areas. However, the formation of clear trabeculae within the SFBC is not visible when compared with native trabecular bone (Fig. 1*F*, cut face).

To get a more detailed overview on the matrix composition, assorted histological and immunohistochemical stainings were applied. Cells were homogenously distributed within the SFBCs as indicated by H&E staining, while Alizarin Red S and von Kossa staining confirmed the deposition of calcium and phosphate, respectively, throughout the tissue (Fig. 2*A*). Interestingly, SFBCs that showed less von Kossa staining exhibited a more pronounced layer-like structure, while the layers itself were strongly mineralized at the borders (Fig. 2*A*; lower row). Negative controls were cultivated without osteogenic medium (Fig. 2*B*). In addition, we observed the expression of *collagen type I* (Col I) and *alkaline phosphatase* (ALP), which are typical markers for osteogenic processes, whereas no Col II, a typical marker of chondrogenesis, was found (Fig. 2*C*).

### SFBCs show profound expression of bone-specific markers

To confirm the previous findings regarding the expression of bone-specific markers, immunofluorescence staining for osteopontin (OPN) and osteocalcin (OC), two non-collagenous bone matrix proteins, were analyzed and yielded the evenly distributed, distinct protein expression (Fig. 3*A*, *B*). Although OPN is mainly produced by immature osteoblasts, OC is a marker of

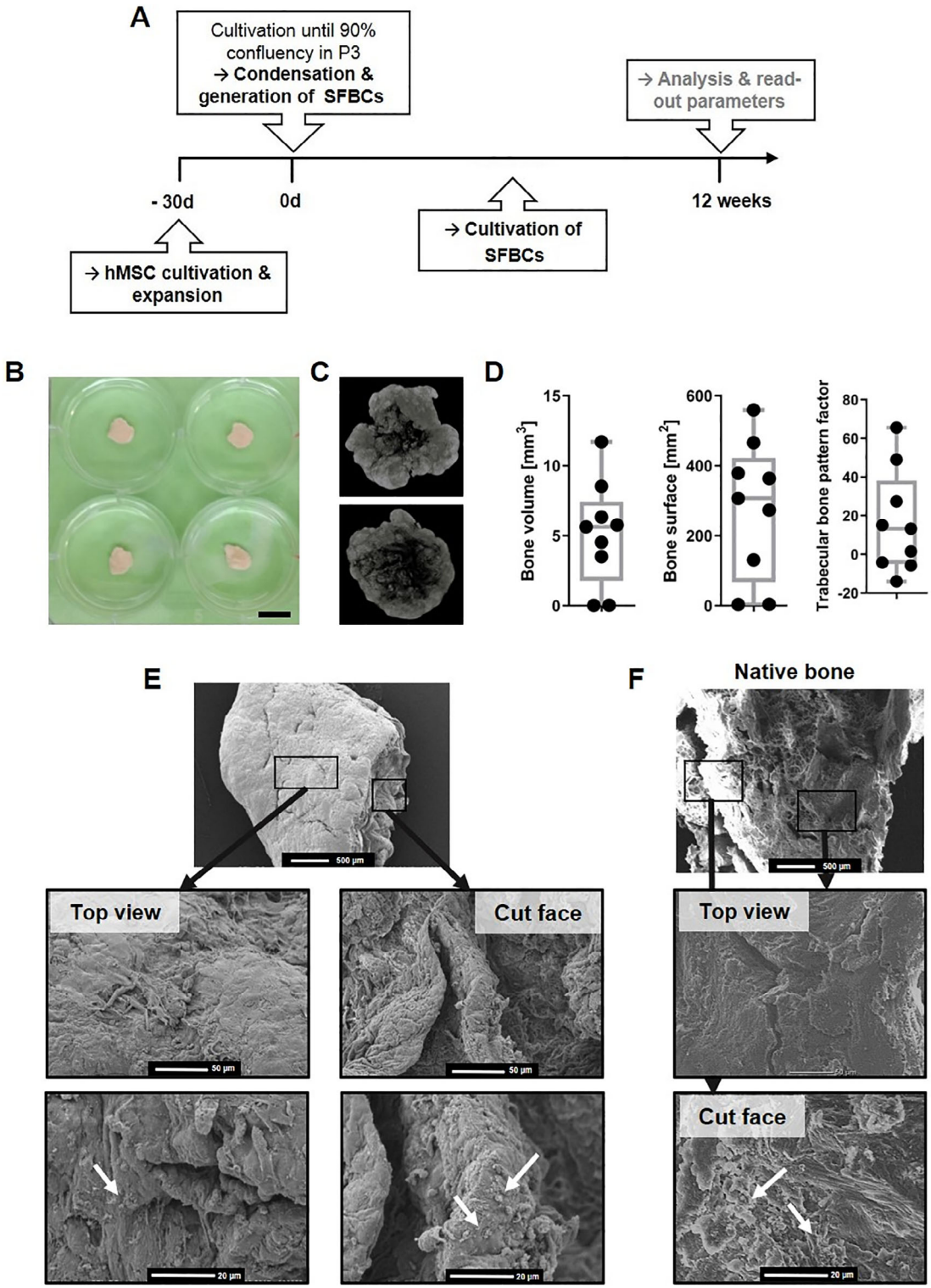


**Fig 1.** Characterization of the SFBCs with respect to mineralization and structure. (*A*) Study design. (*B*) Exemplary images of SFBCs. Scale bar = 1 cm. (*C*) 3D reconstruction of µCT. Exemplary images of $n = 9$. (*D*) Quantitative results from µCT analysis. Data are shown as box plots with median, interquartile range, max and min values, and all data points. $n = 9$. (*E*) Structural/morphological examination of the SFBCs in comparison to (*F*) human native cortical (top view)/trabecular bone (cut face) using scanning electron microscopy. Exemplary images of $n = 3$ SFBCs and $n = 2$ native human bone pieces. Scale bars are indicated in the images. Arrows mark isolated crystal-like depositions.

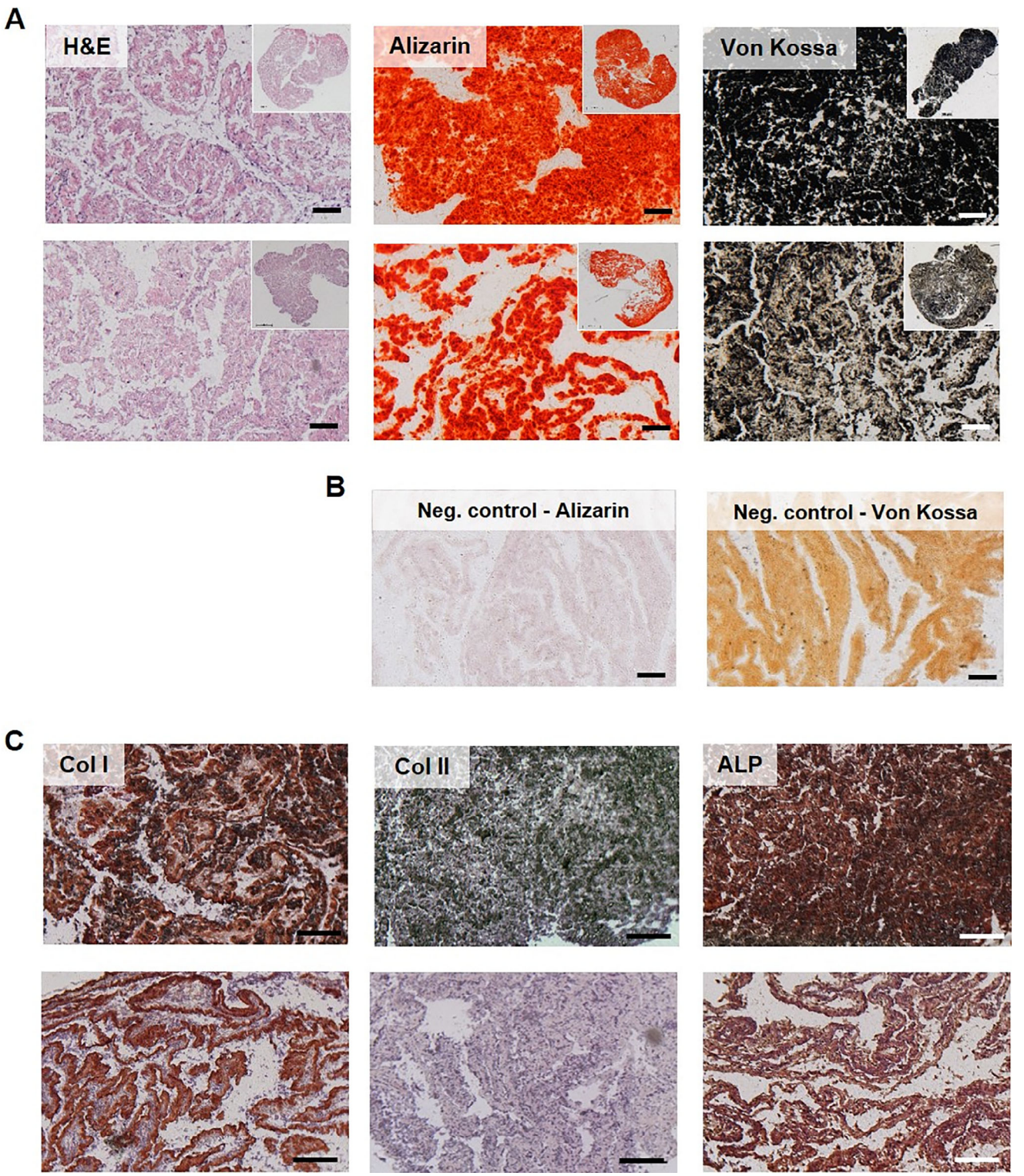


**Fig 2.** Histological and immunohistochemical examination of the SFBCs. (*A*) Exemplary images of H&E, Alizarin red staining, and von Kossa stains. Upper row is exemplary for fully calcified SFBCs and lower row for less fully calcified SFBCs. $n = 9$. (*B*) Negative control for Alizarin red and von Kossa staining. (*C*) Immunohistochemical stainings for Col I, Col II, and ALP. All scale bars = 200 μm. All images are exemplary for $n = 9$.

late-stage osteoblasts, indicating the presence of different cell states within the SFBCs. mRNA expression analysis showed high levels of osteogenic marker genes such as *secreted phosphoprotein 1* (*SPP1*) and *distal-less homeobox 5* (*DLX5*; Fig. 3*C*). *SPP1* was significantly higher expressed (10-fold), whereas *DLX5* was higher expressed by trend (8-fold) when

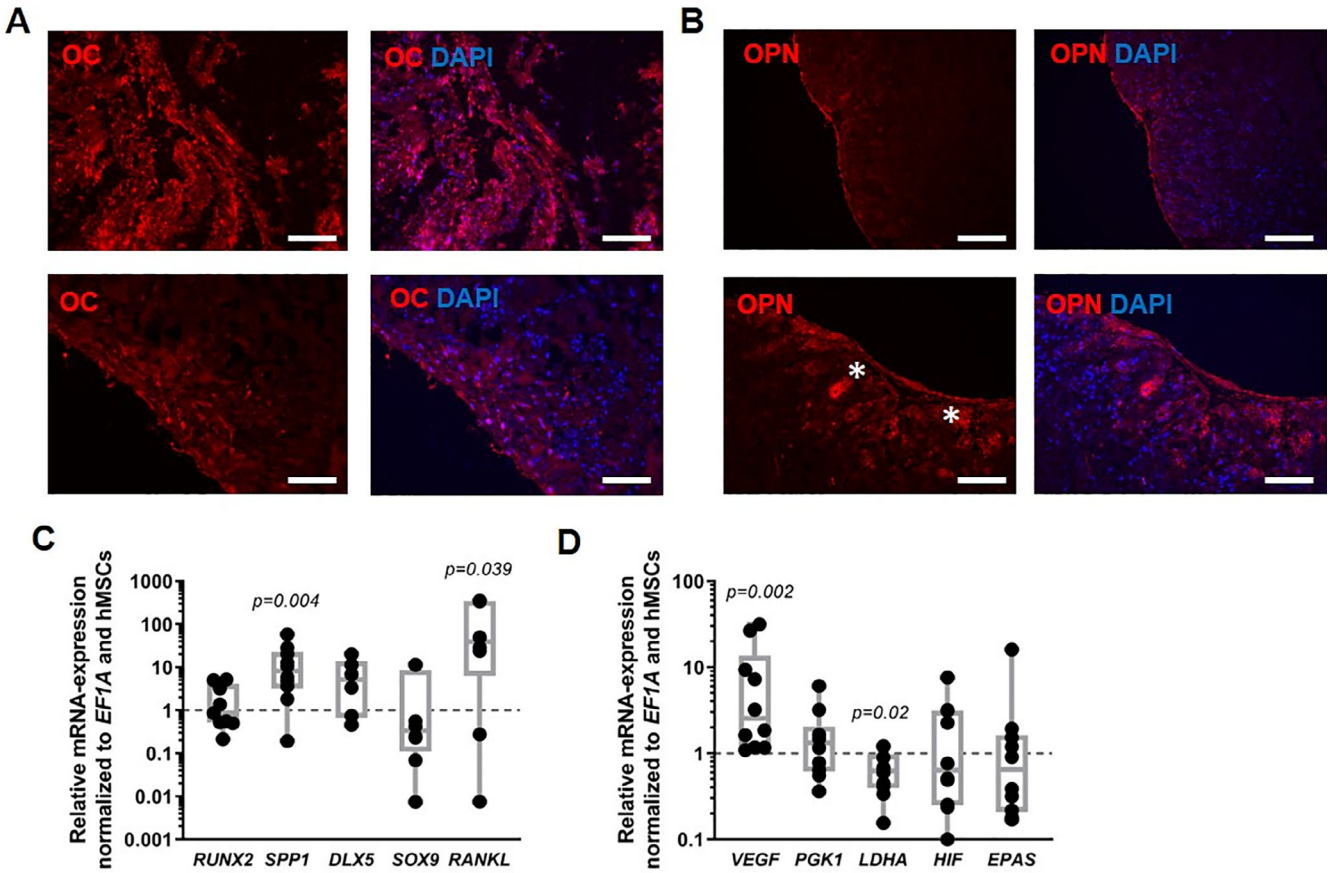


**Fig 3.** Immunofluorescence and mRNA expression analysis of SFBCs. (*A*, *B*) Immunofluorescence staining of osteocalcin (OC; *A*) and osteopontin (OPN; *B*). White asterisks highlight cells with high OPN production. To reveal the nuclei of present cells, all slides were counterstained with DAPI. All scale bars = 200 μm. Images are exemplary for $n = 3$. (*C*) qPCR results of mature osteogenic markers (*SPP1*, *DLX5, RANKL*) ($n = 8$–10), and (*D*) metabolic marker *VEGFA* is highly expressed while other metabolic markers (*PGK1, LDHA, HIF1, EPAS*) and markers indicative for osteoprogenitors (RUNX2, SOX9) remain at a basal level ($n = 10$). Data are shown as box plots with median, interquartile range, max and min values, and all data points. For statistical analysis, the results were compared with the expression level of monolayer hMSC, and the Wilcoxon signed rank test was used (Supplemental Table S3).

compared with monolayer MSCs. In contrast, the early osteogenic transcription factor *runt-related transcription factor 2* (*RUNX2*) and the chondrogenic marker *SRY-box transcription factor 9* (*SOX9*) were expressed on a more basal level. Interestingly, *receptor activator of NF-κB ligand* (*RANKL*) was highly expressed (Fig. 3*C*). Moreover, *vascular endothelial growth factor* (*VEGF*) was significantly higher expressed (10-fold), although other hypoxia-inducible factor (HIF1) target genes such as *phosphoglycerate kinase 1* (*PGK1*), *lactate dehydrogenase A* (*LDHA*), *endothelial PAS domain-containing protein 1* (*EPAS*), and *HIF1* were comparably or lower (*LDHA*) expressed as in monolayer MSCs (Fig. 3*D*).

## Co-cultivation indicates biological functionality of SFBCs

To confirm the functionality of the SFBCs and to mimic the initial phase of fracture healing in an adequate experimental setting, SFBCs were directly co-cultivated with FH models under hypoxic conditions (5% $CO_2$, ~ 1% $O_2$) for 12 hours up to 48 hours (Fig. 4*A*), since the initial phase of fracture healing in humans takes place within the first 72 hours.[2] However, preliminary results indicated a significant loss of living cells within the FH models after an incubation of 72 hours (Supplemental Fig. S1).

Although we have not fixed both models to each other by any technical measures, we observed a close contact of the FH with the corresponding SFBC, allowing direct cell–cell contact and cross-talk between the models. After co-cultivation for 48 hours, H&E staining revealed the typical cell morphology with no obvious alterations within the SFBCs, whereas the cells in the FH seemed to be evenly distributed. The calcification throughout the SFBC was reconfirmed via von Kossa staining with no obvious calcification in the border areas of the FH (Fig. 4*B*). We have previously shown that the most interesting observations in our in vitro FH were visible between 12 and 48 hours with respect to immune cell survival and activity.[16] Thus, in a first experiment, mRNA expression in the FH and the SFBC was analyzed after 12 and 48 hours and normalized to the mean expression at 0 hours (Fig. 4*C*, *D*, respectively). Analysis of the mRNA expression in the FH indicated a time-consistent, upregulated expression of *RUNX2, SPP1, MMP2, VEGF, LDHA*, and *PGK1* with only numerical differences between time points—except for *LDHA* (Fig. 4*C*). The main differences were observed for the inflammatory markers *interleukin 6* (*IL6*) and *IL8*, which were slightly lower

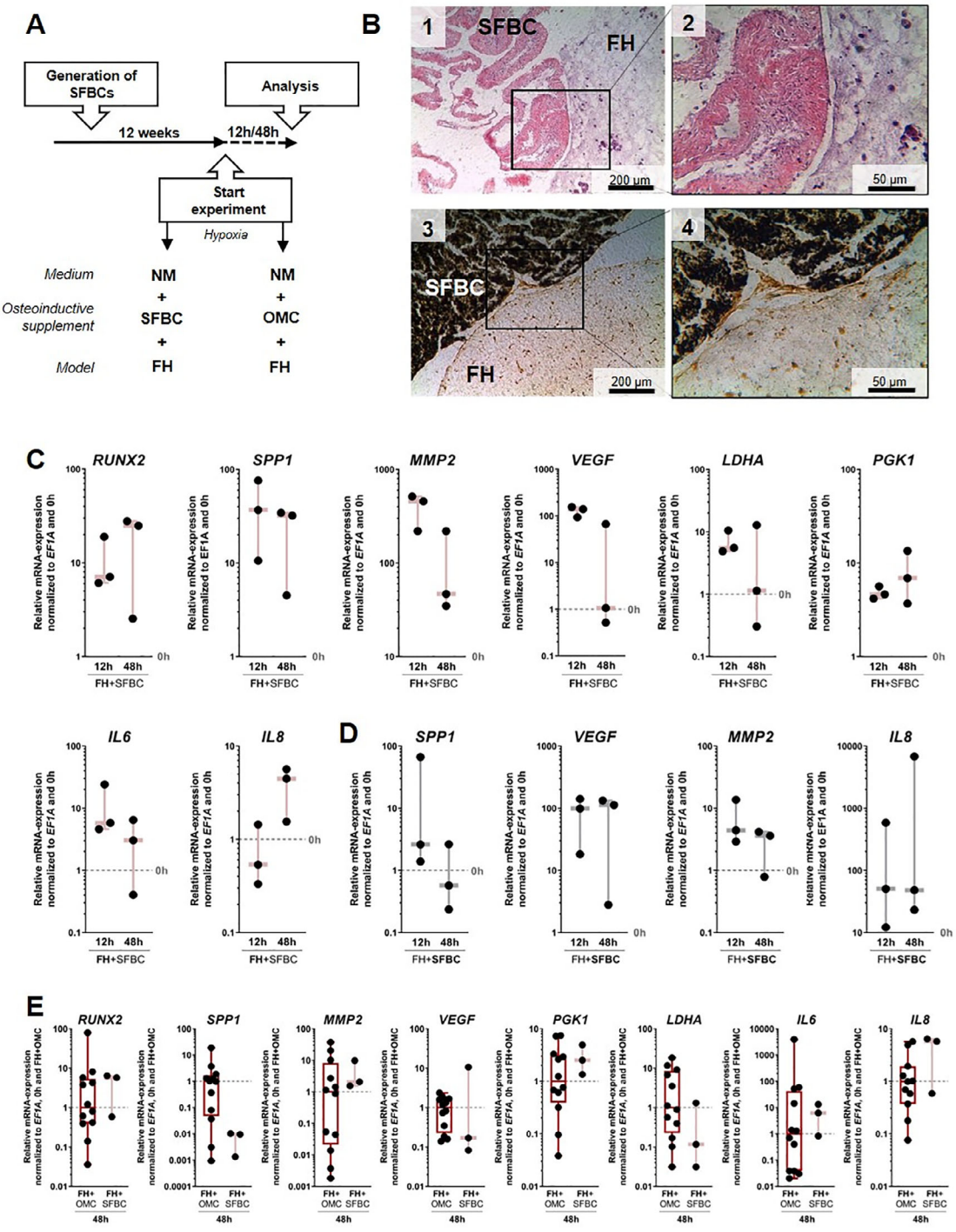


**Fig 4.** Co-cultivation of SFBCs and in vitro FH. (*A*) Experimental setup for the co-cultivation study. NM = normal cultivation medium; OMC = osteogenic medium components. (*B*) Exemplary images of H&E (1, 2) and von Kossa staining (3, 4). Images in the right row (2, 4) are magnifications. Scale bars are indicated. (*C*) qPCR results of the FH model after 12- and 48-hour co-cultivation with SFBCs under hypoxic conditions. Data are normalized to *EF1A* and 0 hour to verify induction of gene expression by co-cultivation. Data are presented as individual data points with median, max and min values ($n = 3$). Statistical significance was determined using the Wilcoxon signed rank test (matched pairs and unpaired to hypothetical value = 1; Supplemental Tables S4 and S5). (*D*) qPCR results of the SFBCs after 12- and 48-hour co-cultivation with FH under hypoxic conditions. Data are normalized to *EF1A* and 0 hour. Data are presented as individual data points with median, max and min values ($n = 3$). Statistical significance was determined using the Wilcoxon signed rank test (matched pairs and to hypothetical value = 1; Supplemental Tables S6 and S7). (*E*) qPCR results of the FH model after 12- and 48-hour co-cultivation with SFBCs compared with the FH + OMC control. Data are normalized to *EF1A*, 0 hour, and the median of FH + OMC. Data are presented as box plots with median, interquartile range, max and min values, and all data points ($n = 3$–12). Statistical significance was determined using the Mann–Whitney test (unpaired; Supplemental Table S8).

expressed after 48 or 12 hours, respectively. Within the SFBCs, *SPP1* was elevated after 12 hours and was marginally lower expressed at 48 hours compared with 0 hours (Fig. 4*D*). *MMP2*, *VEGFA*, and *IL8* were highly expressed at both time points.

Based on these data, further expression analysis and experiments were conducted after 48 hours of co-cultivation. To verify the biological functionality, in particular the osteoinductive potential of the SFBC, we compared the results from the co-cultivated FH model with a FH + OMC control group (treated only with osteogenic medium components [OMC]: β-glycerophosphate, ascorbic acid, dexamethasone). The normalization of the data to the starting point (0 hours) and the FH + OMC control revealed no substantial differences between both groups (Fig. 4*E*). Only *SPP1* was lower expressed in the FHs co-cultivated with SFBCs compared with the FH + OMC control. Based on these findings, we concluded that the SFBCs show a comparable osteoinductive capacity as the OMC and, therefore, biological functionality. Control experiments investigating the effect of the medium composition (± OMC) on the FH and SFBC revealed only slight differences between the groups regarding *MMP2* and *LDHA* expression after 48 hours in the FH and a time-dependent upregulation of *IL8* within the FH when supplementing OMC (Supplemental Figs. S2 and S3).

Regarding the protein release, we confirmed the secretion of the pro-inflammatory IL-6 and the pro-inflammatory/-angiogenic IL-8. The pro-inflammatory GM-CSF and MIP-1β were also released (Fig. 5*A*). All other analyzed cytokines could not be measured because of concentrations lower than the detection level.

### DFO treatment intensifies pro-angiogenic processes

For evaluation of the model suitability to identify interfering substances, we supplemented 250 μM DFO for 48 hours and analyzed the changes in mRNA expression and protein release. DFO is an iron chelator, which inhibits prolylhydroxylases to chemically stabilize HIF and is a well-known osteoinductive substance.[20] After co-cultivation for 48 hours and supplementation of DFO, we found that DFO triggered the expression of osteogenic, angiogenic, and hypoxia-related genes in the in vitro FH with barely any effect on the SFBCs (Fig. 5*B*). In detail, the expression of the osteogenic marker *SPP1* in the FH was higher expressed compared with the untreated control, whereas DFO had no effect on the expression of *RUNX2*. The inflammatory markers *MMP2* and *IL6* were additionally elevated, whereas the pro-angiogenic factor *VEGFA* and the hypoxia-responsive *LDHA* were highly expressed under the influence of DFO compared to the untreated control group (Fig. 5*B*). Referring to the mRNA expression within the SFBCs, we observed a pattern very similar to untreated conditions, which were expected because of the short treatment period (Fig. 5*B*). Finally, the protein release of IL-6 and IL-8 was slightly induced after 24 hours with DFO supplementation (Fig. 5*C*). These results confirm the interfering potential of DFO and indicate different response dynamics within the co-cultivation system.

## Discussion

To study the interaction between bone and immune cells within the fracture gap, adequate in vitro systems should recapitulate cell–cell interactions and the microenvironment (hypoxia). Here, we first developed and characterized SFBCs, which were co-cultivated with FH models under hypoxic conditions to verify the osteoinductive potential of SFBCs and to recapitulate certain aspects of the initial phase of fracture healing. To stratify the model regarding the responsiveness toward potentially interfering substances (eg, therapeutics), DFO was supplemented for 48 hours. Based on our data, we were able to distinctly mimic processes of the initial fracture phase in vitro and highlighted the importance of including the cross-talk between bone and immune cells for preclinical studies. Improved tissue engineering approaches employ mesenchymal condensation as a natural form of 3D self-assembly or self-organization consisting exclusively of the cells and their own produced extracellular matrix (ECM).[21] MSCs from the bone marrow, but also the adipose tissue as well as primary cells (osteoblasts) or induced pluripotent stem cells, have been used depending on the availability and phenotype stability. It has been described that bone marrow–derived MSCs tend to mineralize than undergo chondrogenesis after mesenchymal condensation.[14,22] Several techniques are exerted, such as the use of low-attachment plates to induce spontaneous MSC aggregation, membrane-based aggregation (eg, chitosan), or forced aggregation (via centrifugation).[23]

The applied technique patented by Ponomarev and colleagues[24] exploits the capacity of MSC to undergo mesenchymal condensation on a macroscale level to produce macrotissues in a highly standardized manner without causing necrosis formation in the center.[18] The advantage of such macroscale approaches is the physiologically relevant size, geometry, and low cell number and density compared with the matrix and mechanical properties when compared to, for example, spheroids.[18] However, the generation and examination of these constructs are time-consuming and require high numbers of cells limiting the throughput of the system but enabling the performance of several analyses from one model. Here, we reported the bone-like structure and ongoing calcification/mineralization of the SFBCs that were verified by in vitro μCt (Fig. 1) and histology/immunohistochemistry, showing pronounced expression of ALP and Col I in the absence of Col II (Fig. 2). These findings are comparable to other studies using MSC aggregates analyzed after 1 to 3 weeks.[25,26] The morphology and structure of the SFBCs resemble immature woven bone regarding the body structure. To identify bone-representative cell types, we applied immunofluorescence staining. Because osteoblasts and osteocytes are the characteristic cells in native bone, we stained for OPN as well as OC. OPN, a glycol-phosphoprotein,[27] is mainly expressed in immature osteoblasts and OC can be found in late-stage osteoblasts currently transforming to osteocytes. Thus, we have heterogenic differentiation and maturation states within the SFBCs, indicating a heterogeneous cell population in functional balance. With respect to the mRNA expression, we observed augmented expression of osteogenic relevant markers such as *SPP1*, *DLX5*, *RANKL* and *VEGFA* (Fig. 3). *SPP1*, the coding gene for OPN, is hereby the most distinct upregulated gene, coherent with the expression of OPN within the immunofluorescence staining. Muraglie and colleagues observed comparable trends, including a two- to eightfold increase in OC and OPN expression in MSC aggregates cultivated in low-attachment plates.[28] Because *RUNX2* is an early upstream transcription factor, high expression on mRNA level is expected 3 to 7 days after osteogenic induction.[26] After 3 weeks, the process of ossification and cellular differentiation toward the osteogenic lineage is already in an advanced state.[29,30] *VEGFA* is an essential coordinator, not only of angiogenetic processes and important for fracture healing, but also in the process of endochondral ossification[31] and is known to enhance osteogenic differentiation

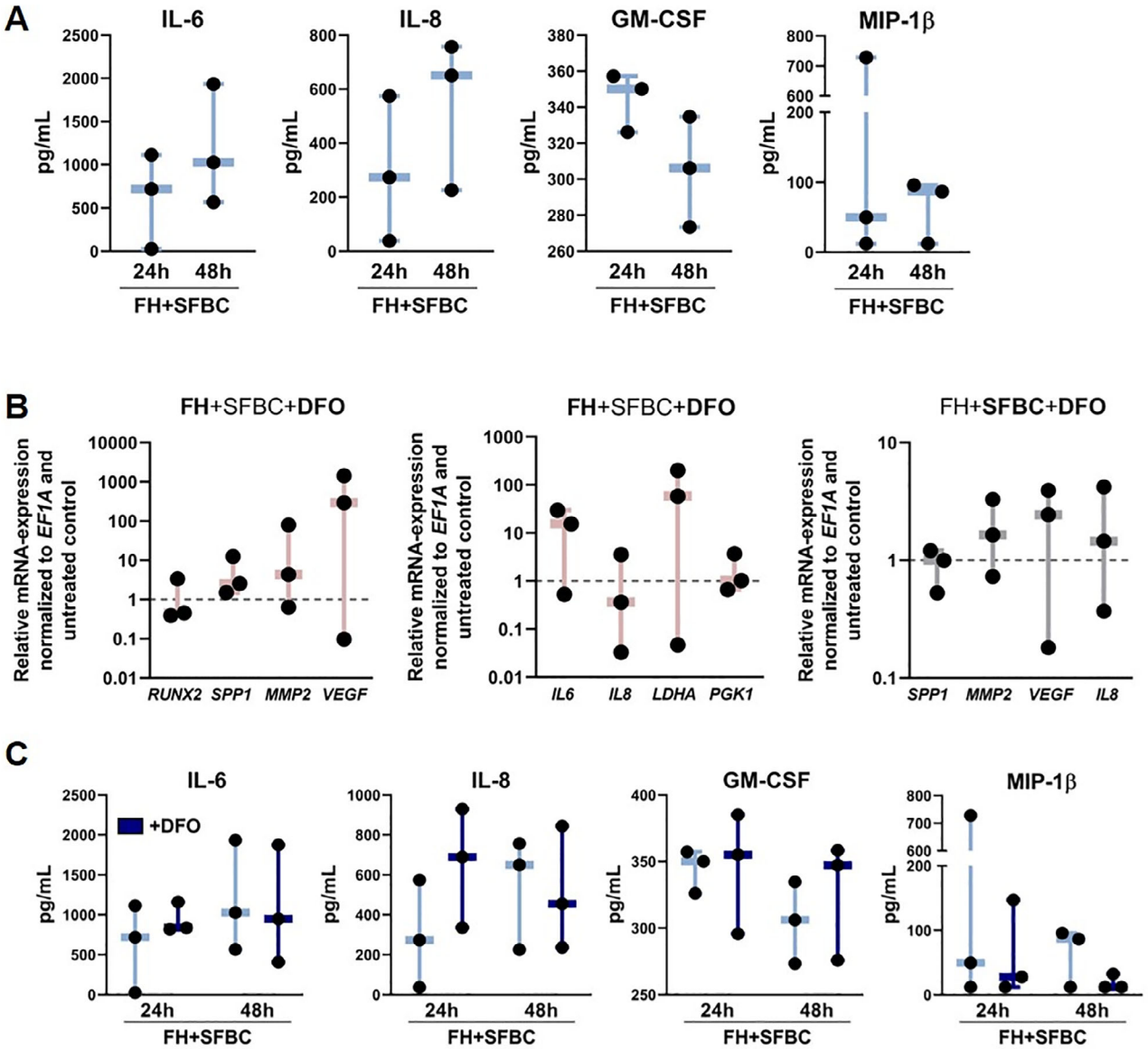


**Fig 5.** Analysis of the supernatant after co-cultivation and co-cultivation of SFBCs and in vitro FH with supplementation of DFO. (*A*) Supernatants were collected after 24 and 48 hours and analyzed via multiplex assay. Statistical significance was determined using the Kruskal–Wallis test with Dunn's multiple comparisons test (Supplemental Table S9). Data are shown as individual data points with median, max and min values. (*B*) qPCR results of the FH or the SFBCs after 48-hour co-cultivation with supplementation of 250 μM DFO (bold abbreviations in title indicate analyzed component). Data are normalized to *EF1A* and the untreated control and presented as individual data points with median, max and min values, and all data points ($n = 3$). Statistical significance was determined using the Wilcoxon signed rank test (Supplemental Tables S10 and S11). (*C*) Supernatants were collected after 24 and 48 hours and analyzed via multiplex cytokine detection assay (dark blue = DFO treated samples). Statistical significance was determined using the Kruskal–Wallis test with Dunn's multiple comparisons test (Supplemental Table S12). Data are shown as individual data points with median, max and min values.

in vitro.[32] Interestingly, other HIF1 target genes such as *PGK1*, *EPAS*, and *HIF1* were comparably expressed as in monolayer MSCs, although *LDHA* was downregulated (Fig. 3*D*). Because the SFBCs were not cultivated under hypoxic conditions, the increased expression of *VEGFA* might result from an alternative pathway, eg, induced by transforming growth factor beta 1 (TGF-β1).[33] *DLX5*, an important transcription factor in osteogenesis and bone development,[34] is also highly expressed within the SFBCs, also indicating an intense ossification process. RANKL is also expressed in mature osteoblasts, differentiating into osteocytes and regulating osteoblastogenesis, indicating the presence of late-stage osteoblasts.[35]

After characterizing their bone-like quantities, we co-cultivated the SFBCs with in vitro FHs to evaluate the osteoinductive

potential and, therefore, the functionality of the SFBCs. Previously, we developed an in vitro FH model, incubated in osteogenic induction medium, which closely reflects the in vivo situation.[16,36] One of the main findings was the importance of hypoxia. Therefore, we included hypoxic conditions in our co-cultivation setup. The co-cultivation of the in vitro FH and SFBCs in NM for up to 48 hours under hypoxic conditions revealed significant initiation of cellular processes (mRNA level) for adaptation to hypoxia and osteogenic induction within the FH (Fig. 4). These findings are in accordance with results from an ex vivo study and an in vitro FH model conducted in our group (Supplemental Table S13).[16,37]

Based on the comparative analysis with an FH + OMC control, we concluded that the SFBCs show a comparable osteoinductive capacity as the OMC and biological functionality indicated by, for example, *VEGF* and *MMP2* (Fig. 4). Interestingly, *SPP1* was noticeably lower expressed in the FH when co-cultivated with SFBCs compared with the FH + OMC control, which could be explained by either the higher amount of OPN provided by the SFBC (Fig. 3) or the considerable high expression/concentration of IL-6 (Figs. 4 and 5*A*), as previously reported.[38] The level of pro-inflammatory cytokines (eg, IL-6 and IL-8) was abundant, which has been also observed in ex vivo samples from patients (Fig. 5*A*).[2,5,37] The microenvironment of the fracture hematoma is described by hypoxia, high lactate and low pH owing to the disruption of vessels, cell death of, for example, erythrocytes, and the lack of nutrients. This cytotoxic environment needs to be counterregulated to allow the invasion of regenerative cells. Therefore, we included whole human blood instead of isolated peripheral blood mononuclear cells (PBMCs). At the initial stage, the microenvironment in the fracture hematoma is acidotic and switched to neutral and slightly alkaline during the regeneration process,[39] which can be triggered by hypoxia. Interestingly, upon co-cultivation, *LDHA* was highly upregulated in the FH model (Supplemental Fig. S2).

Furthermore, the effect of certain immune cells during the initial phase of fracture healing has been studied in detail during the last decade. Lymphocytes play a crucial role as shown in RAG1$^{(-/-)}$ mice supposing a detrimental effect of adaptive immune cells.[40] A negative impact was reported for the presence of CD8$^+$ cytotoxic T cells in humans and mice,[41] whereas CD4$^+$ cells have been shown to enhance osteogenic differentiation in vitro and upregulated osteogenic markers, eg, *RUNX2* or *OC*.[42] This clearly indicates the need to combine bone and immune cells in in vitro approaches to recapitulate the cross-talk, environment, and key features of the in vivo situation.

With respect to the DFO treatment, we found an upregulation of *HIF*-target genes (*VEGFA* and *LDHA*), indicating the effectivity of DFO to stabilize *HIF* (Fig. 5*B*, *C*). In addition, pro-inflammatory processes were more pronounced, which is in accordance with current findings in a mouse-osteotomy model revealing the activation of, for example, *C-X-C motif chemokine ligand* 3 (*Cxcl3*) or *metallothionein 3* (*Mt3*) expression at day 3 after application of DFO in the fracture gap.[20] We did not expect a strong upregulation of osteogenic markers or changes in the SFBCs, which normally require longer treatment periods.[29]

Nevertheless, there are many ways to foster the current approach. To improve the current protocol to generate SFBC, different approaches such as the addition of specific growth factors, eg, BMPs, fibroblast growth factors (FGFs), or VEGFs, enhancing the differentiation and bone formation in vitro can be considered to fasten up the generation period in the future. Furthermore, bioreactors can be used to approximate the environment to the actual in vivo situation by dynamic culturing and restrained environment, while overcoming the lack of nutrient transfer and combining cells with scaffolds.[43] Bioreactors also provide the possibility to withdraw toxic and cell apoptotic signals, perhaps allowing a longer cultivation period of the model. Moreover, to adequately mimic the fracture gap, the adjacent bone marrow might be included within the system to allow the migration of further immune cells but also, for example, endothelial cells, which invade the fracture hematoma to promote neovascularization.

Nevertheless, we present a first approach to recapitulate key features of the initial phase of fracture healing more closely to the in vivo situation by combining macroscale bone equivalents and FH models. Despite some limitations, we here provide data on a prototype of an in vitro fracture gap model that can be used in the future (i) to study potential underlying mechanisms of fracture-healing disorders, eg, using blood of immunologically restricted patients[4,5] to produce the FH models; (ii) to be employed as a prediction tool to identify (potential) interfering substances (eg, glucocorticoids, NSAIDs) or new therapeutics; and (iii) to be further optimized and expanded to provide a sufficient alternative method for active implementation of the 3R principle.

## Disclosures

All authors state that they have no conflict of interests.

## Acknowledgments

The authors thank Manuela Jakstadt for excellent technical assistance. Bone marrow was provided by the "Tissue Harvesting" Core Facility of the Berlin Institute of Health Center for Regenerative Therapies (BCRT). FACS analyses were performed together with the Core Facility at the German Rheumatism Research Centre. AL, FB, AD, MP, and TG are members of Berlin-Brandenburg research platform BB3R and Charité 3$^R$. This study was funded by the German Federal Ministry for Education and Research (BMBF) (project no. 031A334). AL and AD are currently being supported by the Joachim Herz Foundation (Add-on Fellowship 2019/2020). The work of TG was funded by the Deutsche Forschungsgemeinschaft (353142848). Funding bodies did not have any role in designing the study; in collecting, analyzing, and interpreting the data; in writing this manuscript; and in deciding to submit it for publication. Open Access funding enabled and organized by Projekt DEAL.

The authors declare that all data supporting the findings of this study are available within the article and its supplemental information. Further information is made available by the authors upon request.

Author contributions: Moritz Pfeiffenberger: Conceptualization; data curation; formal analysis; investigation; methodology; writing-original draft. Alexandra Damerau: Formal analysis; methodology. Igor Ponomarev: Conceptualization; formal analysis; methodology; resources. Christian Bucher: Formal analysis; methodology; resources; writing-review & editing. Yuling Chen: Formal analysis; methodology. Dirk Barnewitz: Conceptualization; resources; writing-review & editing. Christa Thöne-Reineke: Conceptualization; project administration; supervision; writing-review & editing. Paula Hoff: Conceptualization; writing-review & editing. Frank Buttgereit: Conceptualization; data curation; funding acquisition; project administration; resources; supervision;

writing-review & editing. Timo Gaber: Conceptualization; data curation; project administration; supervision; writing-review & editing. Annemarie Lang: Conceptualization; data curation; formal analysis; writing-original draft; project administration; supervision; writing-review & editing.

## PEER REVIEW

The peer review history for this article is available at https://publons.com/publon/10.1002/jbmr.4267.

## References


1. Bhandari M, Busse JW, Hanson BP, Leece P, Ayeni OR, Schemitsch EH. Psychological distress and quality of life after orthopedic trauma: an observational study. Can J Surg. 2008;51(1):15-22.
2. Hoff P, Gaber T, Strehl C, et al. Immunological characterization of the early human fracture hematoma. Immunol Res. 2016;64(5–6):1195-1206.
3. Oe K, Miwa M, Sakai Y, Lee SY, Kuroda R, Kurosaka M. An in vitro study demonstrating that haematomas found at the site of human fractures contain progenitor cells with multilineage capacity. J Bone Joint Surg. 2007;89(1):133-138.
4. Hoff P, Gaber T, Schmidt-Bleek K, et al. Immunologically restricted patients exhibit a pronounced inflammation and inadequate response to hypoxia in fracture hematomas. Immunol Res. 2011;51(1):116-122.
5. Hoff P, Gaber T, Strehl C, et al. A pronounced inflammatory activity characterizes the early fracture healing phase in immunologically restricted patients. Int J Mol Sci. 2017;18(3):583.
6. Winkler T, Sass FA, Duda GN, Schmidt-Bleek K. A review of biomaterials in bone defect healing, remaining shortcomings and future opportunities for bone tissue engineering: the unsolved challenge. Bone Joint Res. 2018;7(3):232-243.
7. Grundnes O, Reikeras O. The importance of the hematoma for fracture healing in rats. Acta Orthop Scand. 1993;64(3):340-342.
8. Kolar P, Schmidt-Bleek K, Schell H, et al. The early fracture hematoma and its potential role in fracture healing. Tissue Eng Part B Rev. 2010;16(4):427-434.
9. Bernhardt A, Lode A, Peters F, Gelinsky M. Optimization of culture conditions for osteogenically-induced mesenchymal stem cells in beta-tricalcium phosphate ceramics with large interconnected channels. J Tissue Eng Regen Med. 2011;5(6):444-453.
10. Burska AN, Giannoudis PV, Tan BH, Ilas D, Jones E, Ponchel F. Dynamics of early signalling events during fracture healing and potential serum biomarkers of fracture non-union in humans. J Clin Med. 2020;9(2):492.
11. Schlundt C, Schell H, Goodman SB, Vunjak-Novakovic G, Duda GN, Schmidt-Bleek K. Immune modulation as a therapeutic strategy in bone regeneration. J Exp Orthopaed. 2015;2(1):1.
12. Haffner-Luntzer M, Hankenson KD, Ignatius A, et al. Review of animal models of comorbidities in fracture-healing research. J Orthop Res. 2019;37(12):2491-2498.
13. Scheinpflug J, Pfeiffenberger M, Damerau A, et al. Journey into bone models: a review. Genes. 2018;9(5):247.
14. Dickhut A, Pelttari K, Janicki P, et al. Calcification or dedifferentiation: requirement to lock mesenchymal stem cells in a desired differentiation stage. J Cell Physiol. 2009;219(1):219-226.
15. Shih YV, Varghese S. Tissue engineered bone mimetics to study bone disorders ex vivo: role of bioinspired materials. Biomaterials. 2019;198:107-121.
16. Pfeiffenberger M, Hoff P, Thöne-Reineke C, Buttgereit F, Lang A, Gaber T. The in vitro human fracture hematoma model—a tool for preclinical drug testing. ALTEX. 2020;37(4):561-578.
17. Hahn M, Vogel M, Pompesius-Kempa M, Delling G. Trabecular bone pattern factor—a new parameter for simple quantification of bone microarchitecture. Bone. 1992;13(4):327-330.
18. Weber M-C, Fischer L, Damerau A, et al. Macroscale mesenchymal condensation to study cytokine-driven cellular and matrix-related changes during cartilage degradation. Biofabrication. 2019;12:045016.
19. Curtis KM, Gomez LA, Rios C, et al. EF1α and RPL13a represent normalization genes suitable for RT-qPCR analysis of bone marrow derived mesenchymal stem cells. BMC Mol Biol. 2010;11(1):61.
20. Lang A, Helfermeier S, Stefanowski J et al. HIF-stabilization as possible treatment towards fracture healing disorders. bioRxiv. 2020. https://doi.org/10.1101/2020.07.02.182832.
21. DuRaine GD, Brown WE, Hu JC, Athanasiou KA. Emergence of scaffold-free approaches for tissue engineering musculoskeletal cartilages. Ann Biomed Eng. 2015;43(3):543-554.
22. Farrell MJ, Fisher MB, Huang AH, Shin JI, Farrell KM, Mauck RL. Functional properties of bone marrow-derived MSC-based engineered cartilage are unstable with very long-term in vitro culture. J Biomechan. 2014;47(9):2173-2182.
23. Sart S, Tsai A-C, Li Y, Ma T. Three-dimensional aggregates of mesenchymal stem cells: cellular mechanisms, biological properties, and applications. Tissue Eng Part B Rev. 2014;20(5):365-380.
24. Ponomarev IV, Kochneva LM, Barnewitz D. Effect of 3D chondrocyte culturing conditions on the formation of extracellular matrix in cartilage tissue-engineering constructs. Bull Exp Biol Med. 2014;156(4):548-555.
25. Frith JE, Thomson B, Genever PG. Dynamic three-dimensional culture methods enhance mesenchymal stem cell properties and increase therapeutic potential. Tissue Eng Part C Methods. 2010;16(4):735-749.
26. Kabiri M, Kul B, Lott WB, et al. 3D mesenchymal stem/stromal cell osteogenesis and autocrine signalling. Biochem Biophys Res Commun. 2012;419(2):142-147.
27. Standal T, Borset M, Sundan A. Role of osteopontin in adhesion, migration, cell survival and bone remodeling. Exp Oncol. 2004;26(3):179-184.
28. Muraglia A, Corsi A, Riminucci M, et al. Formation of a chondro-osseous rudiment in micromass cultures of human bone-marrow stromal cells. J Cell Sci. 2003;116(Pt 14):2949-2955.
29. Hoshiba T, Kawazoe N, Tateishi T, Chen G. Development of stepwise osteogenesis-mimicking matrices for the regulation of mesenchymal stem cell functions. J Biol Chem. 2009;284(45):31164-31173.
30. Xu J, Li Z, Hou Y, Fang W. Potential mechanisms underlying the Runx2 induced osteogenesis of bone marrow mesenchymal stem cells. Am J Transl Res. 2015;7(12):2527-2535.
31. Gerber HP, Vu TH, Ryan AM, Kowalski J, Werb Z, Ferrara N. VEGF couples hypertrophic cartilage remodeling, ossification and angiogenesis during endochondral bone formation. Nat Med. 1999;5(6):623-628.
32. Zhang Y, Madhu V, Dighe AS, Irvine JN Jr, Cui Q. Osteogenic response of human adipose-derived stem cells to BMP-6, VEGF, and combined VEGF plus BMP-6 in vitro. Growth Factors. 2012;30(5):333-343.
33. Chae KS, Kang MJ, Lee JH, et al. Opposite functions of HIF-α isoforms in VEGF induction by TGF-β1 under non-hypoxic conditions. Oncogene. 2011;30(10):1213-1228.
34. Chung IH, Han J, Iwata J, Chai Y. Msx1 and Dlx5 function synergistically to regulate frontal bone development. Genesis. 2010;48(11):645-655.
35. Nakashima T, Hayashi M, Fukunaga T, et al. Evidence for osteocyte regulation of bone homeostasis through RANKL expression. Nat Med. 2011;17(10):1231-1234.
36. Pfeiffenberger M, Bartsch J, Hoff P, et al. Hypoxia and mesenchymal stromal cells as key drivers of initial fracture healing in an equine in vitro fracture hematoma model. PLoS One. 2019;14(4):e0214276.
37. Hoff P, Maschmeyer P, Gaber T, et al. Human immune cells' behavior and survival under bioenergetically restricted conditions in an in vitro fracture hematoma model. Cell Mol Immunol. 2013;10(2):151-158.
38. Scutera S, Salvi V, Lorenzi L, et al. Adaptive regulation of osteopontin production by dendritic cells through the bidirectional interaction with mesenchymal stromal cells. Front Immunol. 2018;9:1207.

39. Schell H, Duda GN, Peters A, Tsitsilonis S, Johnson KA, Schmidt-Bleek K. The haematoma and its role in bone healing. J Exp Orthop. 2017;4(1):5.
40. El Khassawna T, Serra A, Bucher CH, et al. T lymphocytes influence the mineralization process of bone. Front Immunol. 2017;8:562.
41. Reinke S, Geissler S, Taylor WR, et al. Terminally differentiated CD8(+) T cells negatively affect bone regeneration in humans. Sci Transl Med. 2013;5(177):177ra36.
42. Grassi F, Cattini L, Gambari L, et al. T cell subsets differently regulate osteogenic differentiation of human mesenchymal stromal cells in vitro. J Tissue Eng Regen Med. 2016;10(4): 305-314.
43. Kashte S, Jaiswal AK, Kadam S. Artificial bone via bone tissue engineering: current scenario and challenges. Tissue Eng Regener Med. 2017;14(1):1-14.